Experimental study of zeolitic diffusion by use of a concentration-dependent surface diffusion model

V.J. Inglezakis [a,b,*], M.M. Fyrillas [c]

[a] *The Environment & Resource Efficiency Cluster (EREC), Nazarbayev University, Astana, Kazakhstan*
[b] *Environmental Science & Technology Group (ESTg), Chemical & Materials Engineering Department, School of Engineering, Nazarbayev University, Astana, Kazakhstan*
[c] *Department of Mechanical Engineering, Frederick University, Nicosia, Cyprus*

ARTICLE INFO

ABSTRACT

Surface diffusivity in adsorption and ion exchange processes is probably the most important property studied expensively in the literature but some aspects, especially its dependence on solid phase concentration, is still an open subject to discussion. In this study a new concentration-dependent surface diffusion model, equipped with a flexible double selectivity equilibrium relationship is applied on the removal of Pb^{2+}, Cr^{3+}, Fe^{3+} and Cu^{2+} from aqueous solutions using a natural zeolite. The model incorporates the Chen-Yang surface diffusivity correlation able to deal with positive and negative dependence with surface coverage. The double selectivity equilibrium relationship successfully represents the experimental equilibrium data, which follow Langmurian isotherm type for Pb^{2+}, sigmoidal for Cr^{3+} and Fe^{3+} and linear for Cu^{2+}. The concentration-dependent surface diffusion model was compared with the constant diffusivity surface diffusion model and found to be moderately more accurate but considerably more useful as it provides more insights into the diffusion mechanism. The application of the model resulted in an average deviation of $8.56 \pm 6.74\%$ from the experimental data and an average solid phase diffusion coefficients between 10^{-9} and 10^{-10} cm^2/s. The results showed that the diffusion of metal ions in the zeolite structure is unhindered following the surface diffusion mass transfer mechanism.

1. Introduction

Heavy metals are common constituents of wastewater and many of them are toxic to environment and, therefore, treatment is required prior to disposal or recycling. Heavy metals are non-biodegradable, tend to accumulate in the environment and eventually though the food chain threaten human health. There is a number of methods for the removal of heavy metals from wastewater, namely precipitation, adsorption, ion exchange and membrane separation. Sorption processes (adsorption and ion exchange) are dominant technologies utilized across different industries and they are especially important in water and wastewater sectors (Fu and Wang, 2011). Several materials are used for the removal of heavy metals from wastewater such as resins, carbons, zeolites and clays (Inglezakis et al., 2016, 2010; Stylianou et al., 2016). Zeolites are hydrated porous aluminosilicate minerals that offer good mechanical and thermal properties and surface area for sorption. The most popular zeolite studied is clinoptilolite (Cincotti et al., 2001; Inglezakis et al., 2003; Stylianou et al., 2015; Woinarski et al., 2006). Although literature on zeolites utilization for heavy metals removal is rich, there are only a

few experimental data on solid phase diffusion coefficients and the application of appropriate mass transfer diffusion-based models is rare. The majority of models used are empirical pseudo-first or second order chemical reaction-like models, which ignore the diffusion steps always apparent in adsorption and ion exchange and thus from physical point of view are problematic (V.J. Inglezakis et al., 2018a,b; Sen Gupta and Bhattacharyya, 2011).

Sorption process is comprised of three steps: (1) mass transfer by diffusion from the bulk fluid phase to the solid's external surface (film diffusion), (2) mass transfer by diffusion into the solid phase (intra-particle diffusion) and (3) adsorption (physical or chemical) on the solid's surface. These steps are common in adsorption and ion exchange the difference being the the stoichiometric character of the later (Zagorodni, 2007). Nevertheless, in practical applications both processes are modeled by using the same equilibrium and kinetics equations. Adsorption in porous solids is typically controlled by the intra-particle diffusion step as film diffusion and adsorption steps are much faster processes (Schwaab et al., 2017). Similar is the situation in ion exchange although the overall rate can be controlled by a slow chemical reaction, if such a reaction

---

Table 1

Experimental studies using batch reactors complete constant diffusivity models.

Solid	Adsorbate	Model[1,2]	Isotherm[3]	Reactor	Film mass transfer coefficient[4] (cm/s)	Surface diffusion coefficient (cm²/s)	Reference
Activated carbon	R6G (dye) p-Nitrophenol	TP-HSDM	Freundlich	Batch with stirring	$1*10^{-3}$ (MOD)	$1.3*10^{-10}$ $1.9*10^{-8}$	(Traegner and Suidan, 1989)
Activated Carbon	Pesticides	HSDM	Freundlich	Differential column batch reactor	-	$6.5*10^{-11}$-$5*10^{-10}$	(Baup et al., 2000)
Activated carbon Zeolite (clinoptilolite)	Basic dyes	TP-HSDM	Freundlich	Batch with stirring (50–600 rpm)	5.8–$6.7*10^{-3}$ (MOD)	$1.5*10^{-11}$-$3.3*10^{-9}$	(Meshko et al., 2001)
Activated carbons	Pesticides	TP-HSDM	Freundlich	Differential column batch reactor	-	$2.5*10^{-11}$-$5*10^{-10}$	(Baup et al., 2002)
Anion resin	Bovine serum albumin γ-globulin	PSDM*	Langmuir	Batch with stirring	-	$4.3*10^{-13}$ $1.6*10^{-10}$	(Chen et al., 2003)
Activated carbon	Acid dyes	TP-HSDM*	Langmuir	Batch with stirring	3-$5*10^{-4}$ (MOD)	$4.7*10^{-11}$-$3.3*10^{-10}$	(Choy et al., 2004)
Granular ferric hydroxide	Arsenate	TP-HSDM	Freundlich	Differential column batch reactor	-	$3*10^{-12}$-$6.4*10^{-11}$	(Badruzzaman et al., 2004)
Bone char	Cd, Cu, Zn	TP-b-HSDM*	Sips#	Batch with stirring (400 rpm)	1.3–$2.1*10^{-3}$ (MOD)	3–$8.2*10^{-9}$	(Ko et al., 2005)
Polymeric adsorbents	Levulinic acid	TP-PSDM*	Sips#	Batch with stirring (500–800 rpm)	4.3–$8.9*10^{-3}$ (MW/COR)	$8*10^{-10}$-$2.6*10^{-8}$	(Liu et al., 2006)
Activated carbon	Geosmin	b-HSDM	Freundlich	Batch with stirring	-	$5.8*10^{-8}$	(Matsui et al., 2009)
Activated carbon	Pyridine	TP-PSDM*	Prausnitz–Radke	Rotating basket batch adsorber (100–200 rpm)	0.3–$2.1*10^{-2}$ (MW)	$4.6*10^{-8}$-$3.8*10^{-7}$	(Ocampo-Perez et al., 2010)
Organobentonite	Phenol	TP-HSDM*	Langmuir	Batch with stirring (300–500 rpm)	0.6–$2.4*10^{-2}$ (MW)	4.1–$5.8*10^{-8}$	(Ocampo-Perez et al., 2011)
Activated carbon	Lanfill leachate micropolutants	TP-PSDM	Prausnitz–Radke	Batch with agitation (135 rpm)	$0.7*10^{-4}$-$9.3*10^{-3}$ (MW)	2.8–$8.7*10^{-11}$	(Raúl Ocampo-Pérez et al., 2012a,b)
Activated carbon	Tetracycline	TP-PSDM	Langmuir	Batch with agitation	-	$9.7*10^{-11}$	(R. Ocampo-Pérez et al., 2012a,b)
Activated carbon cloth	Several organics	TP-PDM*	Prausnitz–Radke	Differential column batch adsorber	-	-	(Leyva-Ramos et al., 2012)
Chitosan films	Food dyes	TP-HSDM	Redlich–Peterson	Batch with stirring (80–200 rpm)	1.3–$2.2*10^{-2}$ (MW)	$4.1*10^{-11}$-$2.3*10^{-9}$	(Dotto et al., 2014)
Zeolite (clinoptilolite)	Rhodamine B (dye)	k-PSDM	Langmuir	Rotating basket batch adsorber	-	$3.9*10^{-11}$-$1.2*10^{-10}$	(Castillo-Araiza et al., 2015)
Activated carbons	Tetracyclines	TP-PSDM	Langmuir	Batch with stirring	1.9–$3.2*10^{-3}$ (MW)	$2.6*10^{-8}$ -$1.1*10^{-10}$	(Ocampo-Pérez et al., 2015)
Activated carbon pellets	Acetaminophen	TP-PSDM	Langmuir	Rotating basket batch adsorber (200 rpm)	0.9–$2.3*10^{-3}$ (MW)	0.6–$1.4*10^{-8}$	(Ocampo-Perez et al., 2017)
Activated carbon	Acid Orange 10 (dye)	TP-HSDM*	Freundlich	Batch with stirring (400 rpm)	$8.2*10^{-3}$ (COR)	$2.2*10^{-11}$	(Muthukkumaran and Aravamudan, 2017)
Activated carbon	Pb, Cd, Ni	TP-PSDM	Langmuir	Batch with stirring (150–330 rpm)	0.9–$2*10^{-3}$ (MOD)	3.4–$7.5*10^{-11}$	(Kavand et al., 2017)
Bentonite	Dye	TP-PSDM	Redlich–Peterson	Batch with shaking (150 rpm)	2–$2.9*10^{-3}$ (MW)	0.7–$1.2*10^{-9}$	(Souza et al., 2017)
Activated carbon fabric	Ibuprofen	TP-PDM	Langmuir-Freundlich#	Batch with shaking (250 rpm)	$7.9*10^{-4}$-$2.9*10^{-2}$ (MOD)	-	(Ondarts et al., 2018)
Activated carbons	Ibuprofen	TP-PSDM	Redlich–Peterson	Batch with shaking (125 rpm)	$9.1*10^{-3}$-$1.8*10^{-2}$ (MW)	$3.7*10^{-8}$-$1.8*10^{-9}$	(Fröhlich et al., 2018)
Activated carbon	Metronidazole	TP-PSDM	Prausnitz–Radke	Rotating basket batch adsorber	0.5–$2.8*10^{-2}$ (MW)	$2.7*10^{-8}$ -$2*10^{-10}$	(Díaz-Blancas et al., 2018)

[1] HSDM: homogeneous diffusion model, b-HSDM: branched pore kinetic model, PSDM: heterogeneous pore and surface diffusion model, k-PSDM: PSDM coupled to a chemical reaction, PDM: pore diffusion model. Models with TP prefix include fluid phase resistance (two-phase models).

[2] Studies marked by asterisc (*) perfrorm an analysis of the surface diffusion variability but the correlation is not included in the model.

[3] Isotherms marked with hashtag (#) are S-shaped.

[4] COR: film mass transfer correlation (dimensional approach), MW: initial slope method (Mathews amd Weber method), MOD: diffusion model application.

follows diffusion (Zagorodni, 2007). Analytical solutions to the diffusion-based models are possible under certain conditions such as linear or rectangular isotherm and infinite solution volume (Suzuki, 1990). The analytical and approximate solutions are mostly based on the work of Crank (1975) and those of Boyd et al. (1947), Paterson (1947) and Helfferich (1962). A comprehensive review on the mechanisms and models used in adsorption and ion exchange is provided by Inglezakis et al. (2019) (Inglezakis et al., 2019).

This study presents and evaluates a new versatile diffusion-based adsorption model equipped with a mixed concentration dependence variable diffusivity correlation and an S-shaped equilibrium isotherm.

The model is applied to the removal of heavy metals from aqueous solutions by a natural zeolite. In this kind of systems, there are only two studies employing constant-diffusivity HSDM models, i.e. these of Meshko et al. (2001) and Castillo-Araiza et al. (2015), and none a variable-diffusivity model. Thus, the combined model presented in this paper is for the first time applied in zeolite liquid-phase adsorption.

2. Background

Experimental papers on liquid phase adsorption using batch reactors complete diffusion-based models are summarised in Table 1. Although

Table 2
Experimental studies using batch reactors complete variable diffusivity models.

Solid	Adsorbate	Model	Variable-diffusivity correlation	Isotherm	Reactor	Film mass transfer coefficient (cm/s)	Zero-loading surface diffusion coefficient (cm^2/s)	Reference
Activated carbon	Dye	TP-PSDM	Higashi–Ito–Oishi Neretnieks	BET[#]	Batch with stirring	2.7–5.9×10^{-2} (MOD)	5.2×10^{-10} 1.6×10^{-11}-1.6×10^{-10}	(Leitao et al., 1992)
Activated carbon	Toluene	TP-HSDM	Neretnieks	Fritz–Schlünder[#]	Batch with stirring (300–900 rpm)	6.8×10^{-3}-1.4×10^{-2} (COR)	3.6×10^{-9}	(Chatzopoulos et al., 1993)
Chabazite (zeolite)	Cs, Sr, Ca, Mg	PSDM	Darken	Langmuir	Carberry-type reactor (500–1000 rpm)	-	1.8×10^{-10}-6.4×10^{-9}	(Robinson et al., 1994)
Activated carbon	Pentachlorophenol	TP-HSDM	Hutchinson and Robinson (empirical)	Fritz–Schlünder[#]	Batch with shaking (200 rpm)	5×10^{-3} (MW)	5.5×10^{-11}	(Mollah and Robinson, 1996)
Activated carbon	Dye	TP-HSDM	Neretnieks	Fritz–Schlünder[#]	Batch with stirring (400 rpm)	5×10^{-4} (MOD)	1.2×10^{-11}	(Yang et al., 2003)
Faujasite (zeolite)	p-Xylene o-xylene ethylbenzene (in i-octane)	PSDM	Higashi–Ito–Oishi	Sips[#]	Batch with stirring	-	0.8–4.5×10^{-14}	(Minceva and Rodrigues, 2004)
Activated carbon	Dye	TP-PSDM	Higashi–Ito–Oishi	Langmuir	Batch with shaking (150 rpm)	4.6×10^{-4} (MOD)	9.3×10^{-12}	(Choong et al., 2006)
Silica based sorbents	Cu Pb	TP-HSDM	Higashi–Ito–Oishi	Langmuir	Not available	-	1.2×10^{-12}-9.1×10^{-11} 1.7×10^{-12}-2.4×10^{-8}	(Russo et al., 2015)
Xerogels	Cytochrome c (protein)	TP-HSDM	Marban et al. (empirical)	Redlich–Peterson	Batch with shaking (75–200 rpm)	5×10^{-4} (MOD)	6.5–9.7×10^{-8}	(Marbán et al., 2018)

this is not an exhaustive list, is evident that studies are moslty limited to activated carbons and systems that obey monotonic, aka non-sigmoidal isotherms. A review on fixed beds modeling is presented elsewhere and the main conclusions are the same (V.J. Inglezakis et al., 2018a,b). Also, there are only few experimental studies employing concentration-dependent diffusion-based models as shown in Table 2. This is due to the complexity of the models as non-linear variable diffusivity correlations and equilibrium isotherms are required.

Some studies investigate the variability of surface diffusivity but the analysis is performed on the results of a constant diffusivity model. The constant diffusivity values are correlated with the equilibrium solid phase loading or initial fluid phase concentration, as for example in Hu et al. (2001), Ko et al. (2005) and Ocampo-Pérez et al (Ocampo-Perez et al., 2011, 2010). However, the solid phase loading is increasing from zero to the equilibrium value and the surface diffusivity changes during the transient conditions. Therefore the variable diffusivity correlations must be incorporated into the model equations. Also, it should be noted that in pore diffusion models (PDM and PSDM) the overall (effective) solid phase diffusivity is variable but this is not due to the variability of surface diffusivity, see for example the study of Kavand et al. (2017).

Recently, Marban et al. (Marbán et al., 2018) claimed that the diffusion coefficient depedence on the surface coverage has not been considered in publsihed adsorption kinetic models onto porous solids which is not accurate as according to Table 2 such models have been solved since 1991; however, it is true that no batch adsorption model incorporating a surface diffusivity correlation able to deal with positive and negative dependence with susface coverage has been published. As discussed in paragraph 3.1 surface diffusivity may have positive, negative or mixed concentration dependence with surface coverage, however the inverse concentration dependence has been rarely reported in batch reactor modeling (Liu et al., 2006). This is evident from Table 2 where with the exception of the work of Marban et al. (Marbán et al., 2018) all other studies employ simple variable diffusivity correlations with a positive dependence with surface coverage. While Marban et al. (Marbán et al., 2018) use an empirical correlation, Chen-Yang correlation used in
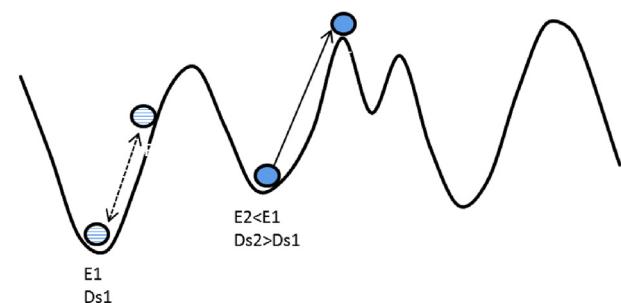

Fig. 1. Diffusion in low and high energy sites.

the present study has a sound theoretical basis and from this point of view is superior.

3. Theory

3.1. Variable surface diffusivity correlations

Mass transport in porous solids occurs in macropores (>50 nm), where pore characteristics are not contributing much, in mesopores (2–50 nm), where surface and capillary forces are important and in micropores (<2 nm) where surface forces are dominant (Choi et al., 2001; Valiullin et al., 2004). In surface diffusion, the transport occurs on the surface of the solid involving jumps between adsorption sites and is an activated process (Ruthven, 1984). In adsorption modeling literature the transport in macropores and mesopores is called pore diffusion, i.e. diffusion in the pore's fluid. In micropores, the diffusion is called configurational or intra-crystalline and shares common characteristics with the surface diffusion (Choi et al., 2001).

For a monolayer surface diffusion, such as molecular diffusion in zeolites without significant pore restriction, the surface diffusivity
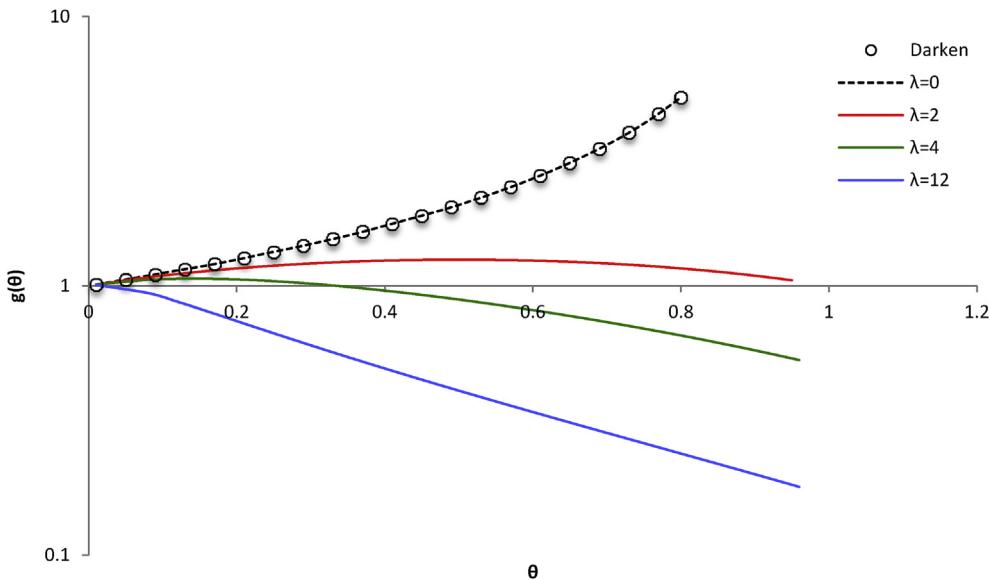
Fig. 2. Effect of (λ) on the surface diffusion coefficient.

normally increases and in some systems decreases with the increase of surface coverage (Chen and Yang, 1998, 1991). At low surface coverage, adsorption occurs on high energy sites where binding of the adsorbed molecules is strong and thus exhibits low mobility (Fig. 1). As the surface coverage increases more lower than high energy sites are available and, because of the weaker binding, molecules diffuse at a faster rate (Do, 1998).

Mass transfer in microporous materials is called configurational or intra-crystalline diffusion and occurs when the pore diameter is close to this of the adsorbate, a typical situation in zeolites. Intra-crystalline diffusion is closer to solid solution than adsorption and is influenced by the molecular size (steric effects) while surface diffusion is a result of thermal motion of the adsorbed molecules (Do, 1998). Thus, strictly speaking, surface and intra-crystalline diffusion are different, but as they share similar features the same mechanism can used for modeling (Choi et al., 2001). This kind of diffusion is called hindered or zeolitic diffusion.

In the present paper we focus on zeolite ion exchange systems and thus only correlations relevant to monolayer movement of adsorbates are discussed. Of the several models published since 1950's this of Chen and Yang (1991) is the most useful as it has theoretical basis and covers both increasing and decreasing trends of the surface diffusion coefficient. The equation is:

$$g(\theta) = \frac{D_s(\theta)}{D_{so}} = \frac{1 - \theta + \frac{\lambda}{2} \cdot \theta \cdot (2 - \theta) + H[1 - \lambda] \cdot (1 - \lambda) \cdot \frac{\lambda}{2} \cdot \theta^2}{\left(1 - \theta + \frac{\lambda}{2} \cdot \theta\right)^2} \qquad (1)$$

where θ is the surface coverage (q/Q_M), Q_M the saturation capacity of the solid, λ is the blockage parameter and H [1-λ] is the Heaviside step function; if $\lambda \geq 1$ then H[$1 - \lambda$] = 0 and if $\lambda < 1$ then H[$1 - \lambda$] = 1. The surface coverage is $\theta = \overline{Y_s} \cdot \overline{Y}$, where $\overline{Y_s} = q_o/Q_M$, $\overline{Y} = q/q_o$ and q_o a reference solid phase concentration (see paragraph 4.1). In the experiments performed in the present study $q_o = Q_M = $ MEL (maximum exchnage level) and thus $\overline{Y_s} = 1$. Eq. (1) as a function of (Y) becomes:

$$g(Y) = \frac{1 - (Y_s \cdot Y) + \frac{\lambda}{2} Y_s \cdot Y \cdot (2 - Y_s \cdot Y) + H[1 - \lambda] \cdot (1 - \lambda) \cdot \frac{\lambda}{2} \cdot (Y_s \cdot Y)^2}{\left(1 - Y_s \cdot Y + \frac{\lambda}{2} \cdot Y_s \cdot Y\right)^2}$$

$$(2)$$

The blockage parameter expresses the degree of pores blocking by the adsorbate. If $\lambda > 0$ hindered diffusion is dominant, as is common in zeolites and if $\lambda = 0$ unhindered surface diffusion drives the mass transfer

(Chen and Yang, 1991). Also, the surface diffusion coefficient is increasing for $\lambda < 1$, has a mixed trend at $\lambda > 1$, and practically decreases with solid loading at $\lambda > 5$ (Fig. 2). Note that Chen-Yang model does not take into account the equilibrium and there is no (λ) that gives g(θ) = 1.

A review of available correlations is provided by Do (1998) and Choi et al. (2001). Chen-Yang variable diffusivity correlation was chosen for modeling in this work as, in contrast to previously published studies, it covers both positive and negative surface coverage dependence.

3.2. Concentration-dependent surface diffusion model

Before introducing the model equations the dimensionless variables are presented. The average dimensionless fluid and solid concentrations at any time (t) are $\overline{X} = \overline{C_t}/\overline{C_o}$ and $\overline{Y} = \overline{q_t}/\overline{q_o}$, where $\overline{C_o}$ is the initial fluid phase concentration at t = 0 and $\overline{q_o}$ is the solid phase concentration in equilibrium with $\overline{C_o}$. I should be noted that any equilibrium point can be used for the normalization of the model, replacing $\overline{q_o}$ and $\overline{C_o}$ in all equations and adapting the initial condition at t = 0 accordingly. The partition ratio (Λ) is (Worch, 2012):

$$\Lambda = \frac{M \cdot \overline{q_o}}{V_L \cdot \overline{C_o}} \qquad (3)$$

where M is the solids mass and V_L the liquid volume. The dimensionless time (T) is:

$$T = \frac{D_{so} \cdot t}{r_p^2} \qquad (4)$$

where r_p is the particles radius. The Biot number is defined as follows (Worch, 2012):

$$Bi = \frac{k_f \cdot r_p \cdot \overline{C_o}}{D_{so} \cdot \rho_p \cdot \overline{q_o}} \qquad (5)$$

where k_f is the liquid film mass transfer coefficient and ρ_p the density of the solid. The material balance is:

$$\overline{Y} = \frac{1}{\Lambda} \cdot (1 - \overline{X}) \qquad (6)$$

where $\overline{Y}$ is the solid phase average concentration (eq. 8). The fluid phase mass transfer is:

$$\frac{\partial \overline{Y}}{\partial T} = 3 \cdot Bi \cdot (\overline{X} - X_{R=1}) \tag{7}$$

By using the material balance we get:

$$\frac{\partial \overline{X}}{\partial T} = -3 \cdot \Lambda \cdot Bi \cdot (\overline{X} - X_{R=1}) \tag{8}$$

The solid phase mass transfer equation is:

$$\frac{\partial Y}{\partial T} = \frac{1}{R^2} \cdot \frac{\partial}{\partial R} \left[R^2 \cdot g(Y) \cdot \frac{\partial Y}{\partial R} \right] \tag{9}$$

where $R = r/r_p$ and (r) the distance from the solid's center. By expanding Eq. (9):

$$\frac{\partial Y}{\partial T} = g(Y) \frac{\partial^2 Y}{\partial R^2} + \frac{\partial g(Y)}{\partial R} \frac{\partial Y}{\partial R} + \frac{2}{R} g(Y) \frac{\partial Y}{\partial R} \tag{10}$$

If surface diffusion coefficient is constant then $D_s(Y) = 1$. The average concentration in the solid phase is:

$$\overline{Y} = 3 \cdot \int_0^1 Y \cdot R^2 dR \tag{11}$$

$$-\frac{2^{1/3} \cdot \left(-a_2^2 + 3a_1 \cdot a_3 \right)}{3a_3 \left(-2a_2^3 + 9a_1 \cdot a_2 \cdot a_3 + 27 \cdot a_3^2 + \sqrt{4 \left(-a_2^2 + 3a_1 \cdot a_3 \right)^3 + \left(-2a_2^3 + 9a_1 \cdot a_2 \cdot a_3 + 27 \cdot a_3^2 \right)^2}\right)^{1/3}}$$

$$+\frac{\left(-2 \cdot a_2^3 + 9a_1 \cdot a_2 \cdot a_3 + 27 \cdot a_3^2 + \sqrt{4 \cdot \left(-a_2^2 + 3a_1 \cdot a_3 \right)^3 + \left(-2a_2^3 + 9a_1 \cdot a_2 \cdot a_3 + 27 \cdot a_3^2 \right)^2}\right)^{1/3}}{32^{1/3} \cdot a_3} \tag{19}$$

By multiplying both terms of the solid mass transfer rate dimensionless Eq. (11) by $3 \cdot R^2$ and integrating by use of Eq. (17), the following equation is derived:

$$\frac{\partial \overline{Y}}{\partial T} = 3 \cdot g(Y_{R=1}) \left(\frac{\partial Y}{\partial R} \right)_{R=1} \tag{13}$$

The initial conditions for $T = 0$ are $\overline{X}_{T=0} = 1$ and $\overline{Y}_{T=0} = 0$. The boundary condition at the center of the solid (R = 0) is:

$$\left(\frac{\partial Y}{\partial R} \right)_{R=0} = 0 \tag{14}$$

At the solid-fluid interface (R = 1), local equilibrium take place:

$$Y_{R=1} = f(X_{R=1}) \cdot X_{R=1} = f^{-1}(Y_{R=1}) \tag{15}$$

Also, for combined solid and fluid phase mass transfer resistances:

$$g(Y_{R=1}) \cdot \left(\frac{\partial Y}{\partial R} \right)_{R=1} = Bi \cdot (\overline{X} - X_{R=1}) \tag{16}$$

The following equation can be used for the calculation of the average surface diffusion coefficient:

$$D_{s,avr} = \frac{D_{so}}{\theta_\infty} \cdot \int_0^{\theta_\infty} g(\theta) d\theta = \frac{D_{so}}{\overline{Y_\infty}} \cdot \int_0^{\overline{Y_\infty}} g(Y) d(Y) \tag{17}$$

where $\theta_\infty = Y_s \cdot \overline{Y}_\infty$. The subscript (∞) denotes average bulk phase concentrations at $t \to \infty$, i.e., after equilibrium is reached. The material balance at equilibrium is:

$$\frac{1}{\Lambda} \cdot (1 - \overline{X}_\infty) = \overline{Y}_\infty = f(\overline{X}_\infty) \tag{18}$$

$f(\overline{X}_\infty)$ is the equilibrium relationship. Solving the above equation for $\overline{X}_\infty$ we get:

$$\overline{X}_\infty = -\frac{a_2}{3\,a_3}$$

where:

$$a_1 = (3 - K_1 - K_2 + K_2 \cdot \Lambda + K_1 \cdot \Lambda \cdot p - K_2 \cdot \Lambda \cdot p) \tag{20}$$

$$a_2 = (-3 + 2 \cdot K_1 + 2 \cdot K_2 - K_1 \cdot K_2 - K_2 \cdot \Lambda + K_1 \cdot K_2 \cdot \Lambda - K_1 \cdot \Lambda \cdot p + K_2 \cdot \Lambda \cdot p) \tag{21}$$

$$a_3 = (1 - K_1 - K_2 + K_1 \cdot K_2) \tag{22}$$

The fractional attainment of equilibrium for a solid phase free of solute at t = 0 is defined as follows (Helfferich, 1962):

$$U(T) = \frac{\overline{q}_T}{\overline{q}_\infty} = \frac{\overline{Y}}{\overline{Y}_\infty} = \frac{\overline{C}_o - \overline{C}_T}{\overline{C}_o - \overline{C}_\infty} = \frac{1 - \left(\overline{X}/\overline{X}_{T=0} \right)}{1 - \left(\overline{X}_\infty/\overline{X}_{T=0} \right)} \tag{23}$$

Besides the diffusion equations presented above an equilibrium relationship is needed to solve the model. There are several models that can be considered but for zeolite adsorption and ion exchange systems

Table 3
Experimental conditions for the kinetics experiments.

Run	Particle size (mm)	Solid mass (g)
Cr		20
Cr_1		10
Cu		20
Cu_1		10
Fe	1.18–1.4	20
Fe_1		10
Pb		20
Pb_1		10
Pb_2	0.8–1	3.33

the inhomogeneous models are of particular importance as they are able to describe multisite (heterogeneous) solid phases. In its simple form, the solid is assumed to be composed of two distinct regions with no interaction between them. The derived model is called double-selectivity model (DSM) (Bricio et al., 1997; Inglezakis et al., 2018a,b; Pepe et al., 2003):

$$Y = p \cdot \frac{K_1 \cdot X}{1 + (K_1 - 1) \cdot X} + (1 - p) \cdot \frac{K_2 \cdot X}{1 + (K_2 - 1) \cdot X} \qquad (24)$$

where (K) are the equilibrium constants and (p) is the proportion of sites on the solid surface, all positive numbers. This equation was derived for monovalent ions exchange but can represent multi-site adsorption, is simple and flexible and able to represent S-Shaped isotherms. The model can be viewed as two-sites Langmurian (Inglezakis et al., 2018a,b):

$$Y = p \cdot \frac{X}{\left(\frac{1}{K_1}\right) + \frac{(K_1 - 1)}{K_1} \cdot X} + (1 - p) \cdot \frac{X}{\left(\frac{1}{K_2}\right) + \frac{(K_2 - 1)}{K_2} \cdot X} \qquad (25)$$

The numerical model was solved on MATLAB by using central differences to spatially discretize the partial differential equations and the modified Euler method to numerically solve the system of ordinary differential equations. The numerical model was validated by comparing its predictions with available analytical solutions found in Crank (1975). To estimate the deviation (error) between the numerical solution and the experimental data the area between the curves was used as the error, which does not depend on the orientation of the curves. A detailed description of the numerical methods is provided elsewhere (Inglezakis et al., 2019).

The application of the models were done by using D_s and k_f and D_o, k_f and λ as fitting variables for the constant and variable diffusivity models,
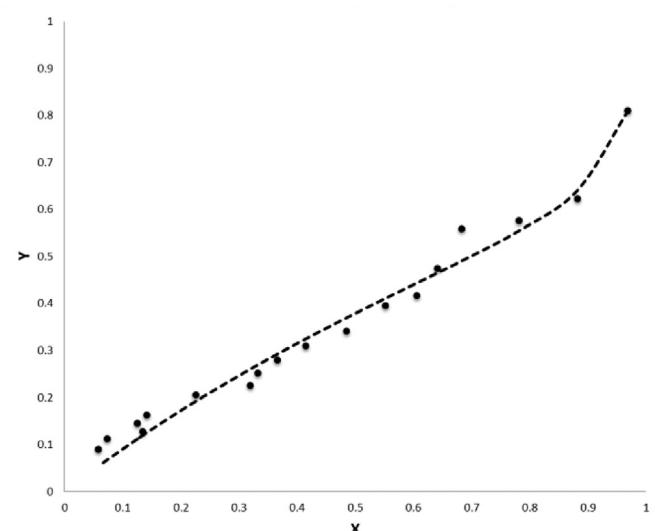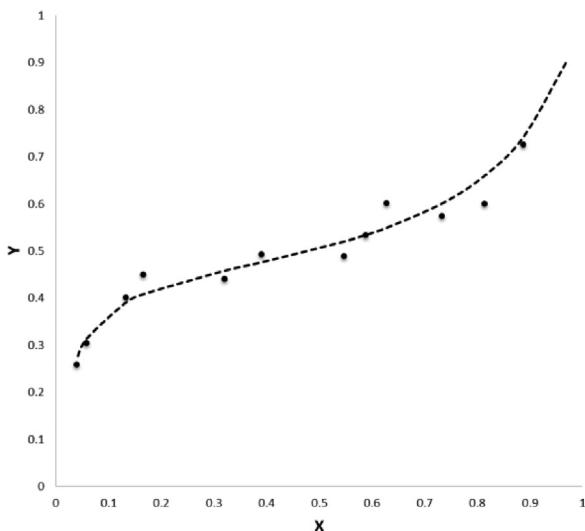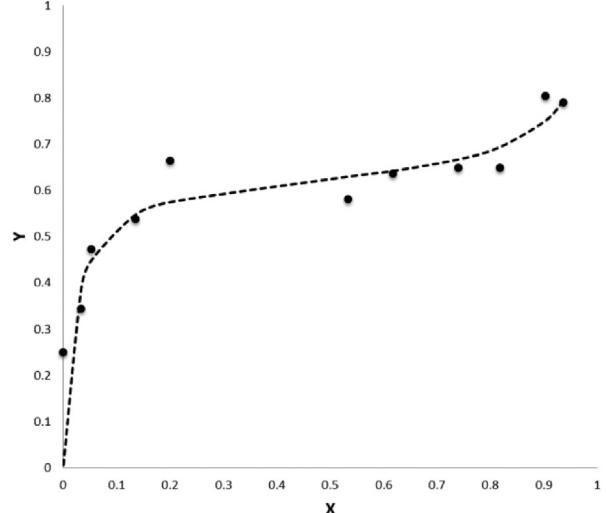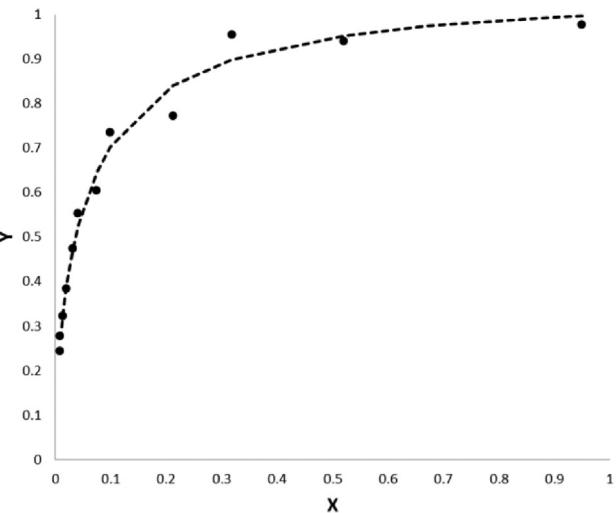

Fig. 3. Isotherms and DSM model fitting: Pb (upper left), Cr (upper right), Fe (lower left) and Cu (lower right).

Table 4
DSM model parameters.

	r	K1	K2	RSS
Pb	0.6326	12.045	121.33	0.004
Cr	0.38	0.058	47.53	0.080
Fe	0.553	0.145	36	0.026
Cu	0.409	0.041	1.596	0.015

Table 5
Minimum values of k_f (cm/s).

Run	Constant diffusivity model (Bi_{min} = 2000)	Variable diffusivity model (Bi_{min} = 200)
Cr	1.41×10^{-2}	7.10×10^{-4}
Cr_1	1.00×10^{-2}	4.44×10^{-4}
Cu	2.77×10^{-2}	1.71×10^{-2} (Bi_{min} = 2000)*
Cu_1	1.85×10^{-2}	1.00×10^{-3}
Fe	4.94×10^{-4} (Bi_{opt} = 196)*	4.28×10^{-4} (Bi_{opt} = 200)
Fe_1	4.40×10^{-3}	8.26×10^{-4} (Bi_{min} = 1000)
Pb	7.22×10^{-3}	4.82×10^{-4} (Bi_{min} = 1000)
Pb_1	8.53×10^{-3}	6.19×10^{-4} (Bi_{min} = 1000)
Pb_2	6.26×10^{-2}	2.23×10^{-3} (Bi_{min} = 500)

* Bi_{min} and Bi_{opt} is the minimum and optimum Biot number, respectively.

respectively. The relative error (%) of the model fit on the experimental

data was calculated as follows:

$$error = 100 \cdot \frac{ABS\left[U(T)_{exp} - U(T)_{mod}\right]}{U(T)_{exp}} \quad (26)$$

where $U(T)_{exp}$ and $U(T)_{mod}$ are the experimental and model U(T) values, respectively. The residual sum of squares (RSS) is used for fitting the DSM model on the experimental equilibrium data:

$$RSS = \sum_{i=1}^{n} \left(Y_{exp.i} - Y_{mod.i}\right)^2 \quad (27)$$

where Y_{exp} and Y_{mod} are the experimental and model solid phase equilibrium concentration values for the same liquid phase equilibrium concentration, respectively. Microsoft's Excel's Solver was used with RSS as the objective function to be minimized.

4. Experimental

The natural zeolite used in this study is clinoptilolite of particles size of 0.8–1.4 mm. The characterization of the material is presented elsewhere (Inglezakis et al., 2002). Equilibrium studies were conducted in 200mL flasks without agitation at 25 °C. Measured quantities of clinoptilolite (0.1–14 g) were mixed with 100 mL metals solutions of 0.01 N
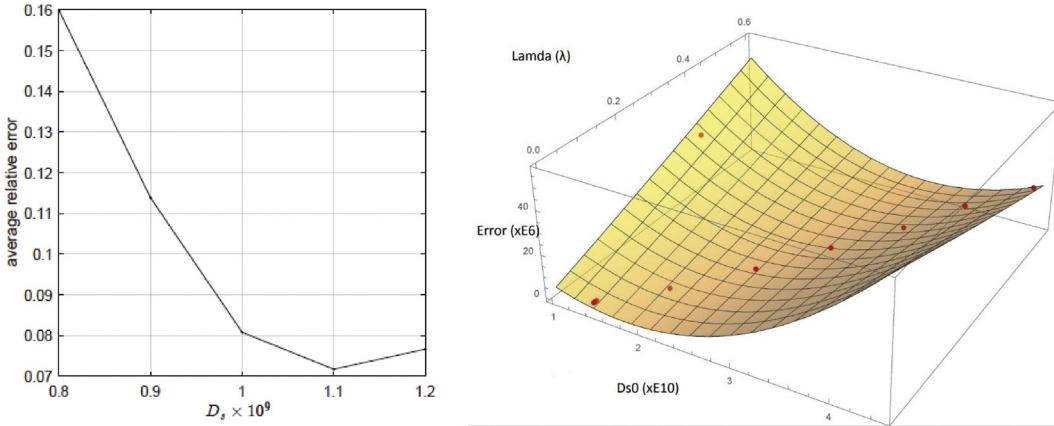

Fig. 4. Error minimization for the constant diffusivity (left) and variable diffusivity (right) model (Pb).
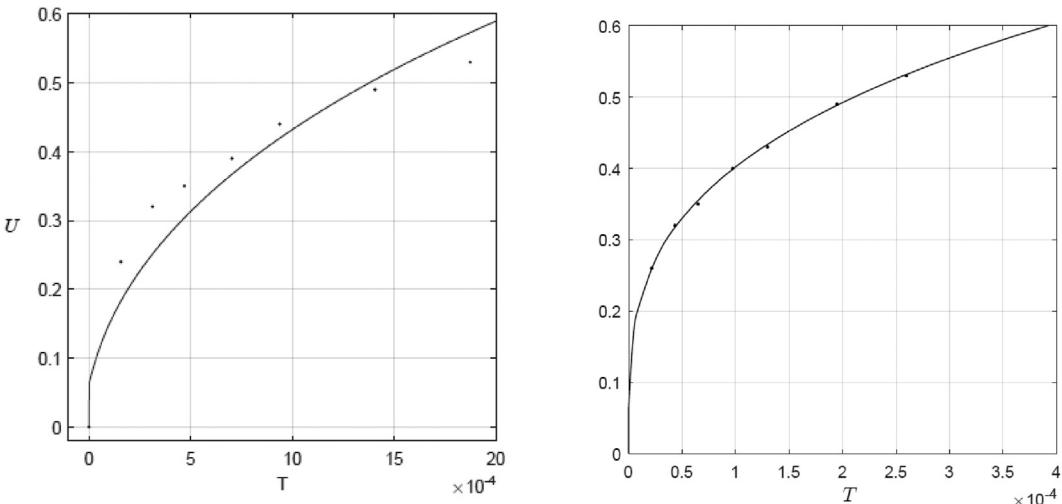

Fig. 5. Characteristic U(T)-T curves for Pb experiment of the constant (left) and variable (right) diffusivity models. The dimensionless time in x-axis is different in the two models.
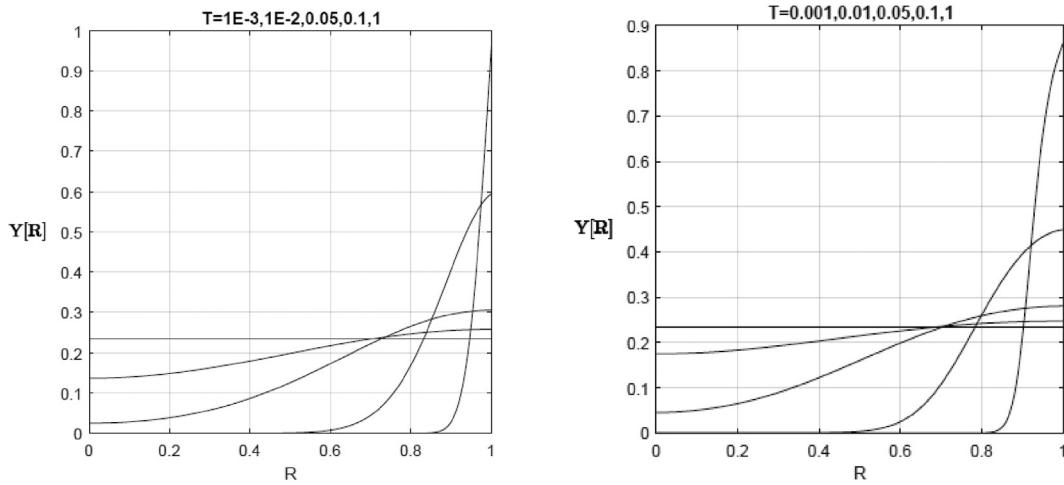
Fig. 6. Characteristic Y(R)-R curves for Pb experiment of the constant (left) and variable (right) diffusivity models.

and initial pH of 4. Every couple of weeks the solution concentration was measured until no further metals removal was observed. Total sampling volume was kept up to 2% of the total solution volume. All experiments were performed at least in duplicate and the average standard deviation was 5%. Kinetic runs were conducted in batch mode where a quantity of zeolite was added in a vessel, containing 500 ml of metal solutions at 0.01 N under rigorous agitation (650 rpm) at 25 °C. Liquid samples were withdrawn at several time intervals and the total sampling volume was kept lower than 1.5% of the total solution volume. pH was initially adjusted to avoid precipitation during all ion exchange experiments, at 4 for Pb^{2+} and Cu^{2+}, 2 for Fe^{3+}, and 3 for Cr^{3+}, using HNO_3. The samples were analyzed for metal ions by AAS, using a Perkin–Elmer Model 350B spectrophotometer. The mean standard deviation of concentration measurements was $1.5 \pm 1\%$. Table 3 presents the experimental runs for the kinetics experiments where two particle sizes of the zeolite were used, namely 0.8–1 and 1.18–1.4 mm. Two runs for each metal were performed by using 3.33, 10 or 20 g of the zeolite.

5. Results and discussion

The DSM application on the experimental equilibrium results is shown in Fig. 3 and Table 4. As is evident, the model is highly flexible and represents the experimental data well.

Although film diffusion is typically much faster than intra-particle diffusion, the film mass transfer coefficient is a key model parameter which influences the overall mass transfer rate. Experimental values of mass transfer coefficients lower than 10^{-3} cm/s can be generally explained by a combination of incomplete mixing and low solid density. However, as is shown in Tables 1 and 2, values in the order of magnitude of 10^{-4} cm/s are frequently reported. Many of these mass transfer coefficients were estimated by the Mathews-Weber method which is suffering from the arbitrary selection of the time where the initial slope is taken which is theoretically at $t = 0$ but practically is calculated for times between 0 and 10 min. In fact in the classic paper of Furusawa and Smith (1973) the authors highlighted the uncertainty associated with the Mathews-Weber method and propose a more general one based on the assumptions of a linear isotherm and absence of intra-particle diffusion at the beginning of the adsorption. In the case of adsorption uptake data, a more accurate method is the application of a complete diffusion model where typically the mass transfer coefficient and the solid phase diffusion coefficient are the fitting variables.

The application of the proposed model showed that the optimum Biot number was always much higher than 100 for both constant and variable

diffusivity models demonstrating that the solid phase diffusion is the mass transfer controlling mechanism. Biot numbers up to 2000 and 200 for the constant and variable diffusivity models were tested, respectively, beyond which the computational time was long and the application of a two-phase model becomes meaningless (see Table 5). These minimum Biot numbers correspond to minimum liquid phase mass transfer coefficients discussed above. Thus, the optimization was made by varying the D_s in the constant diffusivity model and the D_o and λ in the variable diffusivity model (Fig. 4).

Some characteristic examples of the model reults are shoown in Figs. 5 and 6 and the quality of the fit is shown in Fig. 7. The average relative error was $12.54 \pm 9.44\%$ and $8.56 \pm 6.74\%$ for the constant and variable diffusivity models, respectively. As is evident, although the differences are moderate the variable diffusivity model owing to its flexibility provides better predictions. However, its major advantage is the insights it provides into the diffusion process, as discussed below.

The diffusion coefficients derived from the constant diffusivity model are in general agreement with the published data (Table 6). A comprehensive summary on diffusion coefficients in clinoptilolite is provided by Inglezakis et al., (2018 a,b) and for untreated clinoptilolite, diffusion coefficients are generally in the range of 10^{-9}-10^{-10} cm²/s. The available surface diffusivities at zero loading values for liquid phase adsorption on zeolites are rare; values between 1.18–4.20×10^{-9} cm²/s have been reported for dyes adsorption on clinoptilolite (Meshko et al., 2001), 0.18–0.9×10^{-9} cm²/s and 3.00–6.40×10^{-9} cm²/s for Sr, Cs, Ca and Mg ion exchange on two different types of chabazite (Robinson et al., 1994) and 10^{-15}-10^{-14} cm²/s for xylenes adsorption on fausazite (Minceva and Rodrigues, 2004). All diffusion coefficients (D_s, D_{so}, D_{savr}) are following the order Cu > Cr > Fe > Pb. As is evident, especially in the case of Pb, the difference between the D_s given by the constant diffusivity model and $D_{s,avr}$ given by the variable diffusivity model is considerable and thus the diffusion coefficient derived by use of the former provides a very rough approximation of the actual average diffusion coefficient. The blockage parameter (λ) shows some variation for the same metal but it is insignificant as is close to zero indicating the surface diffusion as the controlling intra-particle mass transfer mechanism. An exception is Fe where a value of 0.26 is observed but the overall conclusion is not altered. Moreover, Chen-Yang correlation predicts that for the same D_{so} and unhindered diffusion $D_{s,avr}$ increases with the increase of the surface coverage, which is observed for Pb but not for the other metals probably due to differences in the D_{so} and/or the experimental and model application errors. More data are needed in order to investigate the possible effect of surface coverage on D_{so}.
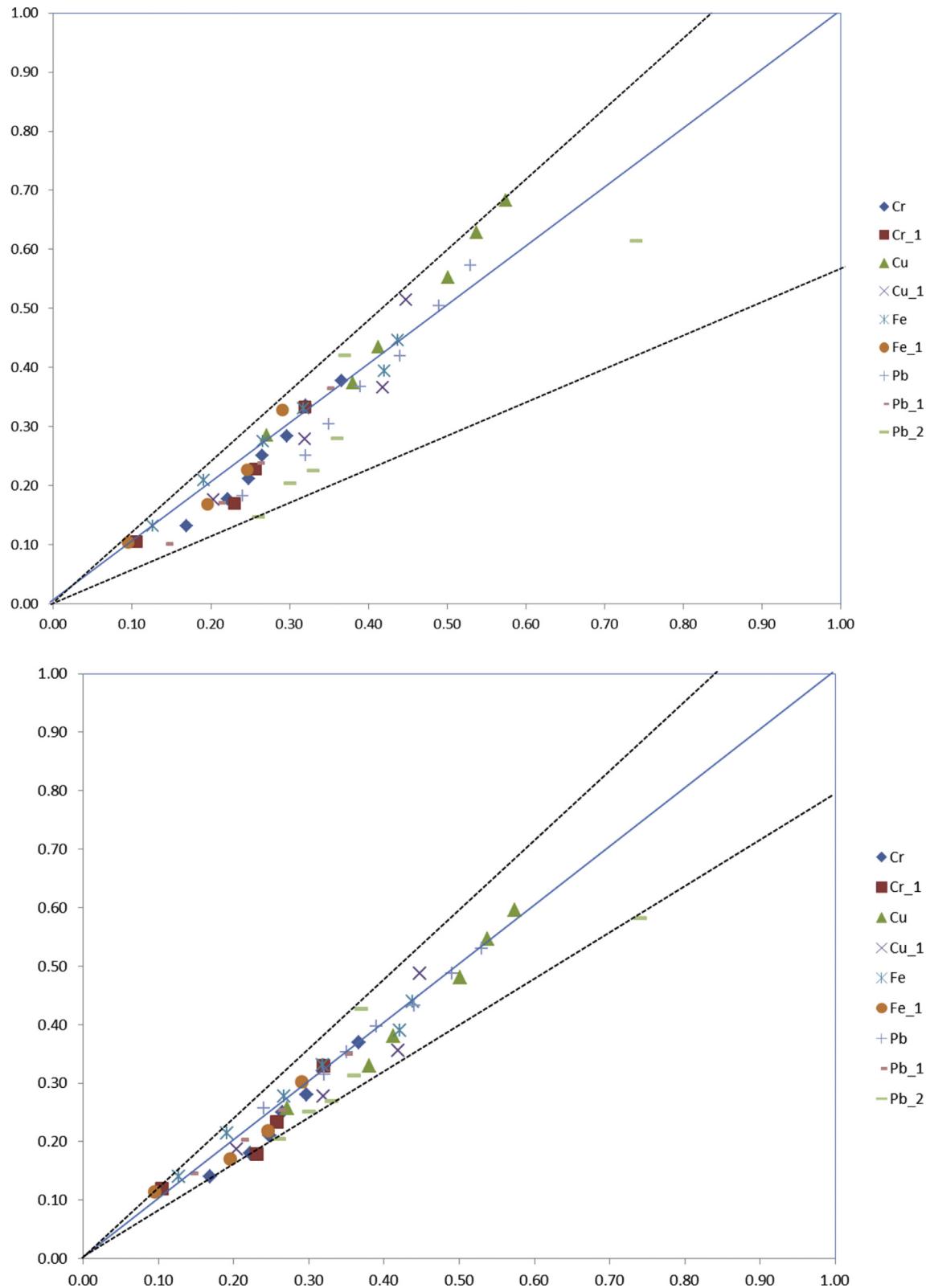
Fig. 7. Model quality: constant diffusivity model (upper) and variable diffusivity model (lower).

Table 6
Results summary.

	Cr	Cr_1	Cu	Cu_1	Fe	Fe_1	Pb	Pb_1	Pb_2
$Ds \times 10^{-9}$ (cm^2/s)	6.00	4.00	11.00	7.80	4.00	2.75	1.10	1.30	5.06
Yoo (mod)	0.56	0.63	0.34	0.45	0.50	0.58	0.23	0.46	0.86
$Dsavr \times 10^{-9}$ (cm^2/s)	4.20	2.83	7.72	4.95	3.40	1.32	0.17	0.24	1.64
$Do \times 10^{-9}$ (cm^2/s)	2.87	1.79	6.32	3.71	2.28	0.88	0.15	0.18	0.72
λ (-)	4.00×10^{-4}	9.00×10^{-3}	10^{-3}	6.00×10^{-6}	0.26	4.00×10^{-3}	0.03	0.01	6.00×10^{-6}

6. Conclusions

A highly flexible homogeneous diffusion model was applied on the kinetics data of Pb^{2+}, Zn^{2+}, Cr^{3+}, Fe^{3+} and Cu^{2+} adsorption on clinoptilolite. The model incorporates the Chen-Yang surface diffusivity correlation and the double selectivity equilibrium equation. The studied systems follow Langmurian isotherm type for Pb^{2+}, sigmoidal for Cr^{3+} and Fe^{3+} and linear for Cu^{2+}. The concentration-dependent surface diffusion model was compared with the constant diffusivity surface diffusion model and found to be moderately more accurate. The concentration-dependent surface diffusion model average deviation from the experimental data is $8.56 \pm 6.74\%$ and the average solid phase diffusion coefficients between 10^{-9} and 10^{-10} cm^2/s. All diffusion coefficients (D_s, D_{so}, D_{savr}) are following the order Cu > Cr > Fe > Pb. The application of the model showed that the uptake rate is controlled by the intra-particle diffusion with a very low blockage parameter, which indicates unhindered surface diffusion mechanism. Further experiments are needed to investigate the apparent variability of the blockage parameter and surface diffusion coefficient at zero loading.

Declarations

Author contribution statement

V. J. Inglezakis: Conceived and designed the experiments; Performed the experiments; Analyzed and interpreted the data; Contributed reagents, materials, analysis tools or data; Wrote the paper.

M. M. Fyrillas: Analyzed and interpreted the data; Contributed reagents, materials, analysis tools or data.

Funding statement

Competing interest statement

The authors declare no conflict of interest.

Additional information

No additional information is available for this paper.

References

Badruzzaman, M., Westerhoff, P., Knappe, D.R.U., 2004. Intraparticle diffusion and adsorption of arsenate onto granular ferric hydroxide (GFH). Water Res. 38, 4002–4012.

Baup, S., Jaffre, C., Wolbert, D., Laplanche, A., 2000. Adsorption of pesticides onto granular activated carbon: determination of surface diffusivities using simple batch experiments. Adsorption 6, 219–228.

Baup, S., Wolbert, D., Laplanche, A., 2002. Importance of surface diffusivities in pesticide adsorption kinetics onto granular versus powdered activated carbon: experimental determination and modeling. Environ. Technol. 23, 1107–1117.

Boyd, G.E., Schubert, J., Adamson, A.W., 1947. The exchange adsorption of ions from aqueous solutions by organic zeolites. Ion-exchange equilibria. J. Am. Chem. Soc. 69, 2818–2829.

Bricio, O., Coca, J., Sastre, H., 1997. Effect of the heterogeneity of macroporous styrene-Dvb resins on ion-exchange equilibria. Solvent Extr. Ion Exch. 15, 647–664.

Castillo-Araiza, C.O., Che-Galicia, G., Dutta, A., Guzmán-González, G., Martínez-Vera, C., Ruíz-Martínez, R.S., 2015. Effect of diffusion on the conceptual design of a fixed-bed adsorber. Fuel 149, 100–108.

Chatzopoulos, D., Varma, A., Irvine, R.L., 1993. Activated carbon adsorption and desorption of toluene in the aqueous phase. AIChE J. 39.

Chen, W.D., Dong, X.Y., Bai, S., Sun, Y., 2003. Dependence of pore diffusivity of protein on adsorption density in anion-exchange adsorbent. Biochem. Eng. J. 14, 45–50.

Chen, Y.D., Yang, R.T., 1998. Surface and mesoporous diffusion with multilayer adsorption. Carbon N. Y. 36, 1525–1537.

Chen, Y.D., Yang, R.T., 1991. Concentration-dependence of surface-diffusion and zeolitic diffusion. AIChE J. 37, 1579–1582.

Choi, J.G., Do, D.D., Do, H.D., 2001. Surface diffusion of adsorbed molecules in porous media: monolayer, multilayer, and capillary condensation regimes. Ind. Eng. Chem. Res. 40, 4005–4031.

Choong, T.S.Y., Wong, T.N., Chuah, T.G., Idris, A., 2006. Film-pore-concentration-dependent surface diffusion model for the adsorption of dye onto palm kernel shell activated carbon. J. Colloid Interface Sci. 301, 436–440.

Choy, K.K.H., Porter, J.F., McKay, G., 2004. Film-surface diffusion during the adsorption of acid dyes onto activated carbon. J. Chem. Technol. Biotechnol. 79, 1181–1188.

Cincotti, A., Lai, N., Orrù, R., Cao, G., 2001. Sardinian natural clinoptilolite for heavy metals and ammonium removal: experiment and modeling. Chem. Eng. J. 84, 275–282.

Crank, J., 1975. The Mathematics of Diffusion, second ed. Clarendon Press, Oxford.

Díaz-Blancas, V., Ocampo-Pérez, R., Leyva-Ramos, R., Alonso-Dávila, P.A., Moral-Rodríguez, A.I., 2018. 3D modeling of the overall adsorption rate of metronidazole on granular activated carbon at low and high concentrations in aqueous solution. Chem. Eng. J. 349, 82–91.

Do, D.D., 1998. Adsorption Analysis: Equilibria and Kinetics.

Dotto, G.L., Buriol, C., Pinto, L.A.A., 2014. Diffusional mass transfer model for the adsorption of food dyes on chitosan films. Chem. Eng. Res. Des. 92, 2324–2332.

Fröhlich, A.C., Ocampo-Pérez, R., Diaz-Blancas, V., Salau, N.P.G., Dotto, G.L., 2018. Three-dimensional mass transfer modeling of ibuprofen adsorption on activated carbon prepared by sonication. Chem. Eng. J. 341, 65–74.

Fu, F., Wang, Q., 2011. Removal of heavy metal ions from wastewaters: a review. J. Environ. Manag. 92, 407–418.

Furusawa, T., Smith, J.M., 1973. Fluid—particle and intraparticle mass transport rates in slurries. Ind. Eng. Chem. Fundam. 12, 197–203.

Helfferich, F.G., 1962. Ion Exchange. Dover science books.

Hu, X., Qiao, S., Zhao, X.S., Lu, G.Q., 2001. Adsorption study of benzene in ink-bottle-like MCM-41. Ind. Eng. Chem. Res. 40, 862–867.

Inglezakis, V.J., Doula, M.K., Aggelatou, V., Zorpas, A.A., 2010. Removal of iron and manganese from underground water by use of natural minerals in batch mode treatment. Desalin. Water Treat. 18, 341–346.

Inglezakis, V.J., Fyrillas, M.M., Park, J., 2019. Variable di ff usivity homogeneous surface di ff usion model and analysis of merits and fallacies of simpli ed adsorption kinetics equations. J. Hazard Mater. 367, 224–245.

Inglezakis, V.J., Fyrillas, M.M., Stylianou, M.A., 2018a. Two-phase homogeneous diffusion model for the fixed bed sorption of heavy metals on natural zeolites. Microporous Mesoporous Mater. 266.

Inglezakis, V.J., Loizidou, M.D., Grigoropoulou, H.P., 2003. Ion exchange of Pb^{2+}, Cu^{2+}, Fe^{3+}, and Cr^{3+} on natural clinoptilolite: selectivity determination and influence of acidity on metal uptake. J. Colloid Interface Sci. 261.

Inglezakis, V.J., Loizidou, M.D., Grigoropoulou, H.P., 2002. Equilibrium and kinetic ion exchange studies of Pb^{2+}, Cr^{3+}, Fe^{3+} and Cu^{2+} on natural clinoptilolite. Water Res. 36.

Inglezakis, V.J., Poulopoulos, S.G., Kazemian, H., 2018b. Insights into the S-shaped sorption isotherms and their dimensionless forms. Microporous Mesoporous Mater. 272, 166–176.

Inglezakis, V.J., Stylianou, M.A., Loizidou, M., Zorpas, A.A., 2016. Experimental studies and modeling of clinoptilolite and vermiculite fixed beds for Mn2+, Zn2+, and Cr3+ removal. Desalin. Water Treat. 57, 11610–11622.

Kavand, M., Asasian, N., Soleimani, M., Kaghazchi, T., Bardestani, R., 2017. Film-Pore-[Concentration-Dependent] Surface Diffusion model for heavy metal ions adsorption: single and multi-component systems. Process Saf. Environ. Prot. 107, 486–497.

Ko, D.C.K., Cheung, C.W., Porter, J.F., 2005. A branched pore kinetic model applied to the sorption of metal ions on bone char. J. Chem. Technol. Biotechnol. 80, 861–871.

Leitao, A., da Conceico, E., Santos, R., Rodrigues, A., 1992. Modeling of solid-liquid adsorption: effects of adsorbent loads on model parameters. Can. J. Chem. Eng. 70, 690–698.

Leyva-Ramos, R., Ocampo-Perez, R., Mendoza-Barron, J., 2012. External mass transfer and hindered diffusion of organic compounds in the adsorption on activated carbon cloth. Chem. Eng. J. 183, 141–151.

Liu, B., Yang, Y., Ren, Q., 2006. Parallel pore and surface diffusion of levulinic acid in basic polymeric adsorbents. J. Chromatogr. A 1132, 190–200.

Marbán, G., Ramírez-Montoya, L.A., García, H., Menéndez, J.Á., Arenillas, A., Montes-Morán, M.A., 2018. Load-dependent surface diffusion model for analyzing the kinetics of protein adsorption onto mesoporous materials. J. Colloid Interface Sci. 511, 27–38.

Matsui, Y., Ando, N., Sasaki, H., Matsushita, T., Ohno, K., 2009. Branched pore kinetic model analysis of geosmin adsorption on super-powdered activated carbon. Water Res. 43, 3095–3103.

Meshko, V., Markovska, L., Mincheva, M., Rodrigues, A.E., 2001. Adsorption of basic dyes on granular activated carbon and natural zeolite. Water Res. 35, 3357–3366.

Minceva, M., Rodrigues, A.E., 2004. Adsorption of xylenes on faujasite-type zeolite: equilibrium and kinetics in batch adsorber. Chem. Eng. Res. Des. 82, 667–681.

Mollah, A.H., Robinson, C.W., 1996. Pentachlorophenol adsorption and desorption characteristics of granular activated carbon—II. Kinetics. Water Res. 30, 2907–2913.

Muthukkumaran, A., Aravamudan, K., 2017. Combined Homogeneous Surface Diffusion Model – design of experiments approach to optimize dye adsorption considering both equilibrium and kinetic aspects. J. Environ. Manag. 204, 424–435.

Ocampo-Pérez, R., Abdel daiem, M.M., Rivera-Utrilla, J., Méndez-Díaz, J.D., Sánchez-Polo, M., 2012a. Modeling adsorption rate of organic micropollutants present in

landfill leachates onto granular activated carbon. J. Colloid Interface Sci. 385, 174–182.

Ocampo-Perez, R., Aguilar-Madera, C.G., Dïaz-Blancas, V., 2017. 3D modeling of overall adsorption rate of acetaminophen on activated carbon pellets. Chem. Eng. J. 321, 510–520.

Ocampo-Perez, R., Leyva-Ramos, R., Alonso-Davila, P., Rivera-Utrilla, J., Sanchez-Polo, M., 2010. Modeling adsorption rate of pyridine onto granular activated carbon. Chem. Eng. J. 165, 133–141.

Ocampo-Perez, R., Leyva-Ramos, R., Mendoza-Barron, J., Guerrero-Coronado, R.M., 2011. Adsorption rate of phenol from aqueous solution onto organobentonite: surface diffusion and kinetic models. J. Colloid Interface Sci. 364, 195–204.

Ocampo-Pérez, R., Leyva-Ramos, R., Rivera-Utrilla, J., Flores-Cano, J.V., Sánchez-Polo, M., 2015. Modeling adsorption rate of tetracyclines on activated carbons from aqueous phase. Chem. Eng. Res. Des. 104, 579–588.

Ocampo-Pérez, R., Rivera-Utrilla, J., Gómez-Pacheco, C., Sánchez-Polo, M., López-Peñalver, J.J., 2012b. Kinetic study of tetracycline adsorption on sludge-derived adsorbents in aqueous phase. Chem. Eng. J. 213, 88–96.

Ondarts, M., Reinert, L., Guittonneau, S., Baup, S., Delpeux, S., Lévêque, J.M., Duclaux, L., 2018. Improving the adsorption kinetics of ibuprofen on an activated carbon fabric through ultrasound irradiation: simulation and experimental studies. Chem. Eng. J. 343, 163–172.

Paterson, S., 1947. The heating or cooling of a solid sphere in a well-stirred fluid. Proc. Phys. Soc. 59, 50–58.

Pepe, F., Caputo, D., Colella, C., 2003. The double selectivity model for the description of ion-exchange equilibria in zeolites. Ind. Eng. Chem. Res. 42, 1093–1097.

Robinson, S.M., Arnold, W.D., Byers, C.H., 1994. Mass-transfer mechanisms for zeolite ion-exchange in waste-water treatment. AIChE J. 40, 2045–2054.

Russo, V., Tesser, R., Trifuoggi, M., Giugni, M., Di Serio, M., 2015. A dynamic intraparticle model for fluid-solid adsorption kinetics. Comput. Chem. Eng. 74, 66–74.

Ruthven, D.M., 1984. Principles of Adsorption and Adsorption Processes. John Wiley & Sons.

Schwaab, M., Steffani, E., Barbosa-Coutinho, E., Severo Júnior, J.B., 2017. Critical analysis of adsorption/diffusion modelling as a function of time square root. Chem. Eng. Sci. 173, 179–186.

Sen Gupta, S., Bhattacharyya, K.G., 2011. Kinetics of adsorption of metal ions on inorganic materials: a review. Adv. Colloid Interface Sci. 162, 39–58.

Souza, P.R., Dotto, G.L., Salau, N.P.G., 2017. Detailed numerical solution of pore volume and surface diffusion model in adsorption systems. Chem. Eng. Res. Des. 122, 298–307.

Stylianou, M.A., Inglezakis, V.J., Loizidou, M., 2015. Comparison of Mn, Zn, and Cr removal in fluidized- and fixed-bed reactors by using clinoptilolite. Desalin. Water Treat. 53.

Stylianou, M.A., Inglezakis, V.J., Loizidou, M.D., Agapiou, A., Itskos, G., 2016. Equilibrium ion exchange studies of Zn^{2+}, Cr^{3+}, and Mn^{2+} on natural bentonite. Desalin. Water Treat. 57.

Suzuki, M., 1990. Adsorption Engineering.

Traegner, U., Suidan, M., 1989. Evaluation of surface and film diffusion coefficients for carbon adsorption. Water Res. 23, 267–273.

Valiullin, R., Kortunov, P., Kärger, J., Timoshenko, V., 2004. Concentration-dependent self-diffusion of liquids in nanopores: a nuclear magnetic resonance study. J. Chem. Phys. 120, 11804–11814.

Woinarski, A.Z., Stevens, G.W., Snape, I., 2006. A natural zeolite permeable reactive barrier to treat heavy-metal contaminated waters in Antarctica: kinetic and fixed-bed studies. Process Saf. Environ. Prot. 84, 109–116.

Worch, E., 2012. Adsorption Technology in Water Treatment: Fundamentals, Processes, and Modeling. Walter de Gruyter.

Yang, X., Otto, S.R., Al-Duri, B., 2003. Concentration-dependent surface diffusivity model (CDSDM): numerical development and application. Chem. Eng. J. 94, 199–209.

Zagorodni, A., 2007. Ion Exchange Materials: Properties and Applications, first ed. Elsevier.